

Multiple quantum solid state NMR indicates a parallel, not antiparallel, organization of β -sheets in Alzheimer's β -amyloid fibrils

Oleg N. Antzutkin^{*†}, John J. Balbach^{*}, Richard D. Leapman[‡],
Nancy W. Rizzo[‡], Jennifer Reed^{*}, and Robert Tycko^{*}

^{*}Laboratory of Chemical Physics, National Institute of Diabetes and Digestive and Kidney Diseases, National Institutes of Health, Bethesda, MD 20892-0520

[†]Division of Inorganic Chemistry, Luleå University of Technology, Luleå, Sweden

[‡]Division of Bioengineering and Physical Science, Office of Research Services, National Institutes of Health, Bethesda, MD 20892

Corresponding author:

Dr. Robert Tycko, National Institutes of Health, Bldg. 5, Room 112, Bethesda, MD 20892-0520.
phone: 301-402-8272. fax: 301-496-0825. e-mail: tycko@helix.nih.gov

Proc. Natl. Acad. Sci., in press.

Abstract

Senile plaques associated with Alzheimer's disease contain deposits of fibrils formed by 39-to-43-residue β -amyloid peptides with possible neurotoxic effects. X-ray diffraction measurements on oriented fibril bundles have indicated an extended β -sheet structure for Alzheimer's β -amyloid fibrils and other amyloid fibrils, but the supramolecular organization of the β -sheets and other structural details are not well established because of the intrinsically noncrystalline, insoluble nature of amyloid fibrils. Here we report solid state nuclear magnetic resonance (NMR) measurements, using a novel multiple quantum (MQ) ^{13}C NMR technique, that probe the β -sheet organization in fibrils formed by the full-length, 40-residue β -amyloid peptide ($\text{A}\beta_{1-40}$). Although an antiparallel β -sheet organization is often assumed and is invoked in recent structural models for full-length β -amyloid fibrils, the MQNMR data indicate an in-register, *parallel* organization. This work provides the first site-specific, atomic-level structural constraints on full-length β -amyloid fibrils and is the first application of MQNMR to a problem in structural biology.

Introduction

A variety of peptides and proteins form amyloid fibrils, including those involved in amyloid diseases such as Alzheimer's disease, type II diabetes, and spongiform encephalopathies (1, 2), as well as proteins that are studied primarily as models for the elucidation of fundamental aspects of protein biophysics (3, 4). Compared with monomeric or oligomeric forms of peptides and proteins, relatively little is known definitively about the molecular structure and supramolecular organization of amyloid fibrils. All amyloid fibrils exhibit similar morphologies in electron micrographs (Fig. 1A), despite their diversity of amino acid sequences and sequence lengths. X-ray diffraction measurements on oriented amyloid fibril bundles show a characteristic "cross- β " pattern (2, 5-8), implying an extended β -sheet structure with polypeptide chains running roughly perpendicular to the long axis of the fibril and interchain hydrogen bonds roughly parallel to this axis. This β -sheet structure is supported by recent cryo-electron microscopy measurements (9). Finer structural details are generally not well established because amyloid fibrils are not amenable to structural characterization by single-crystal diffraction and high resolution, liquid state nuclear magnetic resonance (NMR) techniques.

Amyloid fibrils that form senile plaques in Alzheimer's disease are comprised of β -amyloid (A β) peptides that range in length from 39 to 43 residues (10-12). Various shorter fragments of the full-length A β peptides are also known to fibrillize *in vitro* (13-21). A number of structural models for full-length A β fibrils (8, 22-25) and fibrils formed by A β fragments (13-16, 21) have been proposed, most (16, 21-26) but not all (13-15) of which are based on an *antiparallel* β -sheet organization. Here we present solid state ^{13}C NMR data, obtained with novel multiple quantum (MQ) NMR techniques based on time-reversal principles (27-32), that support an extended *parallel* β -sheet organization for fibrils formed by the full-length, 40-residue A β peptide (A β_{1-40}). These data have implications for the development of an understanding of the physical principles that govern fibril formation, and may also contribute to the development of therapeutic agents by structure-based approaches. Our data represent the first reported structural constraints on full-length A β fibrils from solid state NMR, and the first application of MQNMR in structural biology.

The conceptual basis for MQNMR measurements on A β_{1-40} fibrils is depicted in Fig. 1B. Following the isotopic labeling scheme introduced by Lynn, Meredith, Botto and coworkers (13-15), we introduce a single ^{13}C label into the peptide chain. Given that A β_{1-40} fibrillizes in a predominantly β -sheet structure, as supported by fiber diffraction (7, 8), cryo-electron microscopy (9), and infrared spectroscopy (7, 20), the positions of the ^{13}C labels depend strongly on the supramolecular organization within the β -sheets. In an in-register, parallel β -sheet structure, the labels would form a nearly linear chain with internuclear distances of approximately 4.8 Å. In an antiparallel β -sheet structure, the labels would form a nearly planar zig-zag pattern with nearest-neighbor distances that greatly exceed 4.8 Å. If the β -sheets were organized as an antiparallel packing of parallel dimers, as might conceivably occur if certain intermolecular interactions favor a parallel dimerization while other interactions favor antiparallel alignment of the dimers, the labels would be grouped as pairs with a 4.8 Å internuclear distance and with larger distances between pairs. If the β -sheets were constructed from parallel trimers packed in an antiparallel fashion, the labels would occur in linear groups of three. Roughly speaking, a ^{13}C MQNMR spectrum displays signals that arise from NMR transitions (more precisely, coherences) in which a net number n of ^{13}C nuclear spins flip

simultaneously in the magnetic field of the spectrometer, where n is the MQ order (33). For an n -quantum signal to be observable, groups of at least n spins must be linked by a network of nuclear magnetic dipole-dipole couplings, whose strengths are given by coupling constants

$$d = \frac{\gamma^2 \hbar}{2\pi R^3}$$

where γ is the nuclear magnetogyric ratio and R is the internuclear distance.

Moreover, the radio-frequency (rf) pulse sequence used to excite the MQ coherences must be applied for a time τ_{MQ} on the order of $1/d$. Since $d = 70$ Hz for ^{13}C nuclei with $R = 4.8$ Å, when $\tau_{\text{MQ}} \sim 15$ ms one might expect only 1-quantum signals in the antiparallel β -sheet, 2-quantum signals in the dimerized β -sheet, 3-quantum signals in the trimerized β -sheet, and higher-order MQNMR signals in the in-register, parallel β -sheet. These qualitative expectations are made more rigorous in our data analyses, which proceed by quantitative comparisons of experimental MQNMR signal amplitudes with numerical simulations that include couplings among all ^{13}C labels as well as contributions from natural-abundance ^{13}C nuclei.

Methods

Peptide synthesis and fibrillization. Peptides with the human $\text{A}\beta_{1-40}$ amino acid sequence Asp-Ala-Glu-Phe-Arg-His-Asp-Ser-Gly-Tyr-Glu-Val-His-His-Gln-Lys-Leu-Val-Phe-Phe-Ala-Glu-Asp-Val-Gly-Ser-Asn-Lys-Gly-Ala-Ile-Ile-Gly-Leu-Met-Val-Gly-Gly-Val-Val were synthesized on an Applied Biosystems Model 433A peptide synthesizer using standard fluorenylmethoxycarbonyl (Fmoc) protocols with H-benzotriazol-1-yl-tetramethyluronium hexafluorophosphate (HBTU) activation. ^{13}C -labeled alanine was obtained from Cambridge Isotopes and Fmoc-protected by Midwest Biotech. Peptide purity after cleavage from the synthesis resin with a solution of phenol, ethanedithiol, and thioanisole in 95% trifluoroacetic acid and precipitation in t-butylmethylether was approximately 60%, as estimated from electrospray mass spectrometry. Purification to a level of $90 \pm 5\%$ was carried out with preparative reverse-phase high-performance liquid chromatography (HPLC), using a Vydac C18 column and a water/acetonitrile gradient with 0.1% trifluoroacetic acid. Following lyophilization of the HPLC eluent, purified peptides were fibrillized by incubation of unbuffered solutions at 1 mM peptide concentration, 24° C, and pH 7.4 for 5-20 days. Disappearance of monomeric $\text{A}\beta_{1-40}$ was monitored by periodic measurements of the ultraviolet absorption spectrum of aliquots of the incubating solutions after ultrafiltration (Millipore Centricon, 30 kd cutoff). Typically, the absorbance peak at 274 nm due to tyrosine residues dropped to less than 10% of its initial value after three days of incubation. Concomitantly, the solutions became viscous. Fibrillized solutions were then lyophilized for MQNMR measurements. Approximately 10 μmoles of purified, fibrillized $\text{A}\beta_{1-40}$ were obtained from a 0.1 mmol-scale synthesis. Portions of the final MQNMR samples were taken for FTIR, Raman, and optical microscopy measurements. Lyophilized, purified material was used without incubation for control measurements on unfibrillized $\text{A}\beta_{1-40}$.

Evidence for full fibrillization. Because solid state NMR signals include contributions from all $\text{A}\beta_{1-40}$ molecules in the sample, it is important to establish that fibrillized samples do not contain significant quantities of unfibrillized material. Full fibrillization is supported by the following observations: (1) Electron micrographs of material from incubated $\text{A}\beta_{1-40}$ solutions that were subsequently lyophilized for MQNMR measurements show no structures other than fibrils; (2) Optical polarizing microscope images of material from fibrillized MQNMR $\text{A}\beta_{1-40}$ samples show

strong birefringence from more than 90% of the sample volume after staining with Congo Red, including the green birefringence that is characteristic of amyloid. Material from unfibrillized A β ₁₋₄₀ did not stain or show birefringence; (3) Fourier-transform infrared (FTIR) spectra of material from the Ala30-labeled MQNMR sample show a strong amide I band at 1636 cm⁻¹ with a width less than 20 cm⁻¹, as previously reported for undeuterated A β fibrils (20), and Raman spectra show a strong amide I band at 1668 cm⁻¹, also with a width less than 20 cm⁻¹; (4) Conventional, one-dimensional solid state ¹³C NMR spectra of A β ₁₋₄₀ samples, obtained with cross-polarization, high-power proton decoupling, and magic-angle spinning (MAS) at 10 kHz, show characteristic and pronounced changes upon fibrillization. Spectral features generally become significantly sharper, including a reduction in the widths (full widths at half maximum) of the methyl carbon signal at 20 ppm, from a 6.7 ppm to a 2.3 ppm width (in the case of A β ₁₋₄₀ labeled at the methyl carbon of Ala30), and of the natural-abundance carbonyl signal at 172 ppm, from a 5.7 ppm to a 3.7 ppm width. The natural-abundance α -carbon signal develops two distinct peaks at 58.5 ppm and 52.4 ppm upon fibrillization. We interpret these spectral changes empirically as signatures of fibrillization. Samples that do not show these signatures also do not show strong high-order MQ signals.

NMR spectroscopy. NMR experiments were carried out on a Varian/Chemagnetics Infinity-400 spectrometer, operating at a ¹³C NMR frequency of 100.4 MHz. A Varian/Chemagnetics 3.2 mm MAS probe was used for all measurements, although the MQNMR experiments were performed without MAS. MQNMR measurements used the time-reversible rf pulse cycle

$$\left(\frac{\pi}{4}\right)_y \left[-\tau'' - \left(\frac{\pi}{2}\right)_x - \tau' - \left(\frac{\pi}{2}\right)_x - \tau - \left(\frac{\pi}{2}\right)_x - \tau' - \left(\frac{\pi}{2}\right)_x - \tau - \left(\frac{\pi}{2}\right)_{-x} - \tau' - \left(\frac{\pi}{2}\right)_{-x} - \tau - \left(\frac{\pi}{2}\right)_{-x} - \tau' - \left(\frac{\pi}{2}\right)_{-x} - \tau'' \right]_m \left(\frac{\pi}{4}\right)_{-y}$$

described by Suter *et al.* (30) for generation of a single-quantum effective dipole-dipole coupling Hamiltonian during MQ preparation and mixing periods, with cycle time $\tau_c = 4.8$ ms,

total excitation time $\tau_{MQ} = m\tau_c$, $\tau = \frac{\tau_c}{6} - P$, $\tau' = \frac{\tau_c}{12} - P$, and $\tau'' = \frac{\tau_c}{12} - \frac{P}{2}$, where P is the $\pi/2$

pulse length. To average out chemical shifts, four π pulses were inserted in each τ interval and two π pulses in each τ' and τ'' interval as previously described (31, 32). Phases of π pulses followed the sequence -x, -x, x, x. The ¹³C rf amplitude during the multiple pulse cycle was nominally 41.7 kHz, but the lengths of the π , $\pi/2$, and $\pi/4$ pulses were carefully adjusted to maximize the amplitude of 10-, 11-, and 12-quantum signals from polycrystalline L-methionine-*methyl*-¹³C before A β ₁₋₄₀ data were acquired. The multiple pulse cycle was incorporated into a double-resonance technique, with cross-polarization and proton decoupling, as previously described. Proton decoupling fields during the MQ preparation and mixing periods were 140 kHz. ¹³C NMR signals were digitized with a 50 kHz spectral width. To separate signals from different MQ orders, ¹³C pulses during the preparation period were phase-shifted in 32 increments of 11.25°. MQNMR measurements were carried out on 10-15 mg of ¹³C-labeled A β ₁₋₄₀ fibrils. For $\tau_{MQ} = 14.4$ ms, signals were acquired for approximately 100 hours with a recycle delay of 1 s. Extensive block averaging was used to prevent distortions of MQ amplitudes due to drifts in rf amplitudes, probe tuning, or other factors. Data were processed as previously described (31, 32).

NMR simulations. MQNMR excitation spectra were simulated with Fortran programs written specifically for this purpose. These programs calculated the quantum mechanical evolution of

the nuclear spin density operator that describes the state of the spin system under the time-averaged effective dipole-dipole coupling Hamiltonian ideally created by the rf pulse sequence during MQ preparation and mixing periods, using 512 X 512 matrix representations for a nine-spin system, and produced as output the total NMR signal amplitude arising from each order of MQ coherence present at the end of the preparation period. Averaging over 1024 magnetic field directions and natural-abundance ^{13}C configurations (see below) was performed. As controls, simulations that included the experimental rf pulse sequence explicitly as a time-dependent Hamiltonian term were also performed and gave essentially identical results. Simulations of effects of rf inhomogeneity, using the full pulse sequence, indicated that inhomogeneities of $\pm 10\%$ have negligible effects on the relative MQNMR amplitudes. Simulations for linear chains of five, six, and seven spins (plus four, three, and two natural-abundance spins, respectively) revealed no significant changes in the relative MQNMR amplitudes for the τ_{MQ} values used in the experiments. Simulated MQNMR amplitudes for a six-spin chain with nuclear spin polarization initially on the central two spins were not significantly different from simulated amplitudes with all spins initially polarized. These control simulations indicate the adequacy of finite-spin-system simulations for quantitative analysis of the experimental data.

Electron microscopy. Thin carbon films were evaporated from a carbon rod source onto freshly cleaved mica placed on white filter paper in an Edwards Auto 306 coating system, floated off in deionized water, and picked up on lacy Formvar/carbon films (EM Sciences) supported on 200 mesh copper grids. Grids were glow-discharged in air immediately prior to application of 5 μl of fibrillized $\text{A}\beta_{1-40}$ solution at a concentration of 0.5 $\mu\text{g}/\mu\text{l}$. After allowing two minutes for adsorption, grids were washed in deionized water and negatively stained by passing through two drops of 1% uranyl acetate. Excess fluid was blotted off, and grids were dried in air. Transmission electron micrographs were recorded using a Philips/FEI CM120 electron microscope and Gatan GIF100 imaging filter equipped with a cooled slow scan CCD camera.

Results

MQNMR spectra of ^{13}C -labeled $\text{A}\beta_{1-40}$ fibrils are shown in Figs. 2A and 2B for samples labeled at the methyl carbons of alanine residues at positions 21 and 30 in the peptide chain (Ala21 and Ala30). The MQNMR spectra of the two fibrillized samples are strikingly similar, both exhibiting 2-, 3-, and 4-quantum signals detectable above the noise with amplitudes that increase relative to the 1-quantum signal as τ_{MQ} increases. The similarity of the MQNMR spectra of the two fibrillized $\text{A}\beta_{1-40}$ samples is significant because Ala21 is near the midpoint of the 40-residue peptide, while Ala30 is shifted towards the C-terminus. Of the structural models in Fig. 1B, only the parallel β -sheet leads to similar distances (*i.e.*, similar dipole-dipole couplings) among all ^{13}C labels for the two different labeled sites. Thus, even a rudimentary inspection of the MQNMR spectra strongly favors a parallel β -sheet organization over an antiparallel organization.

Control MQNMR spectra of an unfibrillized sample (Fig. 2C) exhibit much weaker MQ signal amplitudes under identical experimental conditions. In Fig. 2C, the 2-, 3-, and 4-quantum amplitudes at $\tau_{\text{MQ}} = 14.4$ ms (relative to the 1-quantum amplitude) are 0.13, 0.01, and 0.00, respectively, in contrast to the values 0.23, 0.05, and 0.02 in Fig. 2B. The 2-quantum and weak 3-quantum signals in the unfibrillized sample are due primarily to couplings of ^{13}C labels to natural-abundance ^{13}C nuclei and couplings among natural-abundance ^{13}C nuclei.

To analyze the MQNMR data in Figs. 2A and 2B quantitatively, MQNMR spectra of nine-spin systems were simulated numerically for the values of τ_{MQ} used in the experiments. In these simulations, six of the spins were placed at positions appropriate for ^{13}C labels in the parallel, antiparallel, dimeric, or trimeric β -sheet models in Fig. 1B, with coordinates determined from an examination of typical β -sheets in protein crystal structures. Specifically, in simulations for Ala30-labeled $\text{A}\beta_{1-40}$ fibrils, the six ^{13}C labels were assigned coordinates $(x_i, y_i, z_i) = (32.0k_i, 4.8i, 1.5k_i)$ in units of \AA , where $i = 1, 2, \dots, 6$. In simulations for Ala21-labeled $\text{A}\beta_{1-40}$ fibrils, the coordinates were $(1.7k_i, 4.8i, 1.5k_i)$. The parallel, antiparallel, dimeric, and trimeric β -sheet models were represented by $(k_1, k_2, k_3, k_4, k_5, k_6) = (0, 0, 0, 0, 0, 0), (-1, 1, -1, 1, -1, 1), (-1, 1, 1, -1, -1, 1), (-1, -1, -1, 1, 1, 1)$, respectively. The x, y, and z coordinates represent displacements along the direction of the peptide chains, the direction of hydrogen bonding between chains, and the direction perpendicular to the β -sheet, respectively. To account for couplings of the ^{13}C labels to nearby natural-abundance ^{13}C nuclei (present at all carbon sites at a 1.1% level), the remaining three spins were positioned randomly within a rectangular box around the six labels with a volume of $1.5 \times 10^4 \text{\AA}^3$, based on an estimated average volume per natural-abundance aliphatic ^{13}C of 5000\AA^3 . Simulated MQ signal amplitudes were averaged over the magnetic field direction relative to the labels and over the random configuration of the three natural-abundance spins. Natural-abundance ^{13}C nuclei that are far from the ^{13}C labels also contribute to the experimental MQNMR signals. Simulations and experiments on unlabeled $\text{A}\beta_{1-40}$ samples indicate that these distant natural-abundance ^{13}C nuclei contribute significantly only to the 1- and 2-quantum signals, with the ratio of 1-quantum to 2-quantum amplitudes being roughly 25:1, 13:1, and 9:1 for τ_{MQ} values of 4.8 ms, 9.6 ms, and 14.4 ms.

Because the experimental MQ amplitudes are not measured on an absolute scale, scaling factors C_{sim} and C_{nat} were adjusted to minimize the total squared deviation between experiments

and simulations
$$s^2 = \sum_{n=2}^5 [A_{\text{exp}}(n; \tau_{\text{MQ}}) - C_{\text{sim}} A_{\text{sim}}(n; \tau_{\text{MQ}}) - C_{\text{nat}} A_{\text{nat}}(n; \tau_{\text{MQ}})]^2, \quad \text{where}$$

$A_{\text{exp}}(n; \tau_{\text{MQ}})$ is the experimental n -quantum signal amplitude for a given τ_{MQ} , $A_{\text{sim}}(n; \tau_{\text{MQ}})$ is the n -quantum signal amplitude from the nine-spin simulations, and $A_{\text{nat}}(n; \tau_{\text{MQ}})$ is the estimated contribution from distant natural-abundance ^{13}C nuclei (nonzero only for $n = 1$ and $n = 2$). One-quantum amplitudes were not included in s^2 because of uncertainty in the $A_{\text{nat}}(1; \tau_{\text{MQ}}) : A_{\text{nat}}(2; \tau_{\text{MQ}})$ ratios that would otherwise dominate the minimization.

Figure 3 shows comparisons of the experimental MQ signal amplitudes with simulations for each β -sheet model in Fig. 1B, *i.e.*, the quantities $A_{\text{exp}}(n; \tau_{\text{MQ}})$ and $C_{\text{sim}} A_{\text{sim}}(n; \tau_{\text{MQ}}) + C_{\text{nat}} A_{\text{nat}}(n; \tau_{\text{MQ}})$. Only the parallel β -sheet model adequately describes all the experimental data, in particular the amplitudes of 3- and 4-quantum signals relative to the 2-quantum signal at all values of τ_{MQ} for both labeling sites. This conclusion is insensitive to the details of the definition of s^2 or the treatment of natural-abundance ^{13}C signals. In the case of Ala30-labeled $A\beta_{1-40}$ fibrils, the trimeric β -sheet model leads to a significantly poorer fit than the parallel β -sheet model, indicating that the parallel organization of the β -sheets extends over at least four peptide chains. The parallel organization may extend to much longer length scales, but this can not be established from our measurements without using much larger values of τ_{MQ} , which would lead to lower overall signal levels and would require excessive signal acquisition times.

^{13}C MQNMR spectra of a fibrillized $A\beta_{1-40}$ sample labeled at the carbonyl carbons of both Val24 and Gly25 were also obtained (data not shown). For this sample, the relative 2-, 3-, and 4-quantum signal amplitudes are 0.28, 0.05, and 0.03 at $\tau_{\text{MQ}} = 9.6$ ms. Simulated amplitudes are 0.27, 0.05, and 0.03, from simulations for six carbonyl labels on three peptide chains in a parallel β -sheet, including effects of the carbonyl chemical shift anisotropy and the full rf pulse sequence. Thus, MQNMR data on this doubly-labeled $A\beta_{1-40}$ sample also support a parallel β -sheet organization.

MQNMR spectra of a fibrillized $A\beta_{1-40}$ sample labeled at the methyl carbon of Ala2 (data not shown) are nearly identical to the spectra of the unfibrillized, Ala30-labeled sample in Fig. 2C. No 4-quantum signals are observed. In addition, the methyl carbon linewidth in the ^{13}C MAS NMR spectrum of the Ala2-labeled sample is 11 ppm, which is significantly greater than the methyl carbon linewidths in fibrillized Ala21- and Ala30-labeled samples. These results indicate that, unlike Ala21 and Ala30, Ala2 is not located in an in-register, parallel β -sheet and may be structurally disordered. Approximately the first ten residues of $A\beta_{1-40}$ are not required for *in vitro* fibrillization (20) and are proteolyzed in fibrils *in vivo* (34). These N-terminal residues are therefore likely to extend outside the β -sheet fibril structure, in agreement with our MQNMR data.

Discussion

Of the models for the supramolecular organization of β -sheets in $A\beta_{1-40}$ fibrils in Fig. 1B, only the in-register, parallel model is consistent with the MQNMR data and simulations presented above. Although acceptable alternative models might conceivably exist, any such models must place Ala21 and Ala30 methyl carbons in groups of at least four with internuclear distances less than approximately 5.5 Å, *i.e.*, $d > 45$ Hz. In an out-of-register, parallel β -sheet, the internuclear distances would depend on the extent of displacement of hydrogen-bonded peptide chains but would exceed 6.0 Å and therefore be inconsistent with the MQNMR data.

Structural models for amyloid fibrils commonly invoke lamination of several β -sheet layers (2, 4-7, 14, 21, 25), with an average spacing between peptide backbones in adjacent laminae of approximately 9 Å in accordance with fiber diffraction results (7, 8). Coupling constants between methyl carbons in adjacent laminae are then expected to be much less than 30 Hz unless the laminae are unusually close together at the labeled site. Given the similarity of the experimental MQNMR spectra of Ala21- and Ala30-labeled A β ₁₋₄₀ fibrils (Fig. 2), omission of possible couplings between ¹³C labels in different laminae in our simulations of MQ signal amplitudes is justified. Couplings between laminae alone can not possibly account for the observed 4-quantum signal amplitudes.

Several molecular-level structural models for full-length A β fibrils have been proposed (22-26). Although very different in detail, all of these models invoke an antiparallel supramolecular organization of β -sheets and are not supported by our MQNMR data. In the A β fibril model of Tjernberg *et al.* (22), Ala21 and Ala30 are located in an intermolecular antiparallel β -sheet and an intramolecular β -hairpin, respectively, leading to distances between ¹³C labels that would exceed 9 Å in our experiments. In the model of Li *et al.* (25), the β -sheet is constructed from antiparallel intermolecular hydrogen bonding of β -hairpins with a turn between residues 25 and 28, leading to a minimum ¹³C-¹³C distance within one β -sheet of approximately 20 Å. In the model of Chaney *et al.* (24), Ala30 is located in an antiparallel β -sheet, leading to a minimum ¹³C-¹³C distance of approximately 9.6 Å, and Ala21 is contained in a dimeric globular domain outside the β -sheet core. In the two-chain, antiparallel β -helix model of Lazo and Downing (23), ¹³C pairs with a separation of roughly 5 Å may be possible, but longer chains of ¹³C labels are not present.

Evidence for antiparallel β -sheets in full-length A β fibrils comes principally from infrared absorption spectra, which show a strong amide I band at roughly 1630 cm⁻¹ and a weak band at roughly 1690 cm⁻¹ that has been interpreted to be characteristic of antiparallel, but not parallel, β -sheets (7, 17, 19, 20, 35). FTIR spectra of our fibrillized MQNMR samples also show these spectral features, suggesting that proper interpretation of the infrared data may be more subtle than previously assumed. Definitive resolution of this issue requires further study, but the following observations may be relevant. First, as discussed below, we do not claim that β -sheets in *all* amyloid fibrils are parallel. Second, our analysis of MQNMR data is based on numerical simulations of the nuclear spin dynamics, which can be carried out accurately and without reference to model compounds or other empirical data. In contrast, the analysis of infrared data is based on experimental spectra (36) or normal mode calculations (37) for model systems that are significantly less complex than β -amyloid peptides. Third, our MQNMR data do not rule out the possibility, suggested by sequence analysis (21), structural models (22-26), liquid state NMR measurements (38, 39), and circular dichroism spectra (20), that fibrillized A β peptides may adopt a conformation that includes intramolecular β -hairpins (20, 22, 23, 25) or other secondary structure elements that may account for the infrared results.

Solid state NMR measurements by Lynn, Meredith, Botto and coworkers (13-15) have established a parallel β -sheet structure for fibrils formed by A β ₁₀₋₃₅, *i.e.*, residues 10 through 35 of A β ₁₋₄₀. Our experimental MQNMR spectra of A β ₁₀₋₃₅ fibrils labeled with ¹³C at the methyl carbon of Ala21 (data not shown) are nearly identical to those of Ala21- and Ala30-labeled A β ₁₋₄₀ fibrils in Fig. 2, supporting the conclusions of Lynn *et al.* and providing additional evidence that the parallel β -sheet organization in A β ₁₀₋₃₅ fibrils extends beyond dimers (13, 14). Lansbury, Griffin and coworkers (16) have reported solid state NMR measurements on

fibrillized A β ₃₄₋₄₂ that support an antiparallel structural model. In addition, MQNMR and rotational-echo double resonance (REDOR) NMR data on amyloid fibrils formed by the peptide N-acetyl-Lys-Leu-Val-Phe-Phe-Ala-Glu-NH₂, *i.e.*, A β ₁₆₋₂₂ with capping groups at the N- and C-termini, indicate an antiparallel β -sheet structure (40). Thus, it appears that amyloid fibrils can exhibit a variety of supramolecular organizations, depending on the specific details of the amino acid composition and sequence.

A common feature of the A β ₁₋₄₀ and A β ₁₀₋₃₅ sequences is the existence of hydrophobic segments (residues 17-21 and 29-40) that are not symmetrically disposed about the midpoint of the peptide chain. As depicted in Fig. 4, an in-register, parallel β -sheet organization juxtaposes the hydrophobic segments of neighboring peptide chains, while an antiparallel organization does not. An in-register, parallel β -sheet organization also juxtaposes charged residues, which might create electrostatic repulsions that destabilize the fibril, but unfavorable electrostatic interactions could be overcome by incorporation of counterions into the fibrils or possibly by interactions between β -sheet laminae. In contrast, A β ₁₆₋₂₂ and A β ₃₄₋₄₂ contain central hydrophobic sequences with a positive charge at the N-terminus and a negative charge at the C-terminus (*i.e.*, the positively charged Lys and negatively charged Glu sidechains in capped A β ₁₆₋₂₂, and the positive amino and negative carboxylate groups at the ends of uncapped A β ₃₄₋₄₂). These two A β fragments therefore resemble simple electric dipoles when in extended conformations. An antiparallel β -sheet organization may then simultaneously juxtapose hydrophobic segments and minimize the electrostatic energy. Simple considerations such as these based on amino acid composition and sequence may help explain the supramolecular organizations adopted by different A β peptides, although the full explanations are undoubtedly more subtle. Additional atomic-level structural constraints from solid state NMR will further elucidate the details of amyloid fibril structures and the physical basis for these structures.

The MQNMR methods employed in this work represent a general approach to investigations of supramolecular organization in amyloid fibrils. Although ¹³C labeling of alanine methyl sites is advantageous because of the relatively small chemical shift anisotropy (CSA) of these sites, the same MQNMR methods are applicable to other sites with larger CSA (32). It is worth noting that the β -sheet helix model for transthyretin fibrils developed by Blake and Serpell (5) is depicted with parallel β -sheets. However, as discussed by Blake and Serpell (5), the supramolecular organization of β -sheets in this model can not be established unambiguously from their synchrotron x-ray diffraction data.

Although A β ₁₋₄₀ accounts for the majority of A β production *in vivo*, A β ₁₋₄₂, with an additional two hydrophobic residues at the C-terminus, is the predominant species in senile plaques and is believed to nucleate plaque formation (11, 41, 42). In light of the small difference in the two peptide sequences and experimental evidence that A β ₁₋₄₀ and A β ₁₋₄₂ can cofibrillize (41-43), it seems likely that A β ₁₋₄₂ and A β ₁₋₄₀ fibrils have the same supramolecular organization.

Acknowledgements

O.N.A. was supported by a fellowship from the Swedish Foundation for International Cooperation in Research and Higher Education. J.R. was supported by the Whitaker Foundation through the NIH Biomedical Engineering Summer Internship Program. We are grateful to Drs. P. McCarthy, H. Wang, and I.W. Levin for carrying out FTIR and Raman measurements on A β

fibril samples and to Dr. L.K. Pannell for mass spectrometry. Simulations were executed on the SGI Origin 2000 computer in the NIH Center for Information Technology.

Figure captions

Figure 1. (A) Electron micrographs of negative-stained A β_{1-40} fibrils adsorbed to carbon films from an A β_{1-40} solution after incubation at 24° C and pH 7.4 for three days. Typical amyloid fibrils are observed, appearing as single filaments or bundles of filaments with overall diameters ranging from 8 to 20 nm and with twist periodicities between 40 and 150 nm. The same solution, in which the A β_{1-40} peptides were labeled with ^{13}C at the methyl carbon of Ala21, was subsequently lyophilized for multiple quantum NMR measurements shown in Fig. 2. (B) A β_{1-40} fibrils are believed to have a predominantly β -sheet structure with peptide chains (blue arrows) approximately perpendicular to and hydrogen bonds approximately parallel to the long axis of the fibril (green arrow). Four candidates for the supramolecular organization of the fibrils are shown. These can be distinguished experimentally by incorporating ^{13}C labels (red dots) at a single site in the peptide and measuring ^{13}C multiple quantum NMR spectra, because observation of an n-quantum signal requires that at least n ^{13}C nuclei be close enough in space to have significant magnetic dipole-dipole couplings.

Figure 2. ^{13}C multiple quantum NMR spectra of fibrillized and unfibrillized A β_{1-40} samples, shown in order of increasing multiple quantum excitation time τ_{MQ} . Each multiple quantum spectrum is displayed as a series of subspectra for multiple quantum orders from 1 to 6, with a spectral window from -15 kHz to +15kHz in each subspectrum. Vertical scales are adjusted so that 1-quantum peaks are clipped at 25% of their maximum values. In the fibrillized samples (A and B), the amplitudes of 2-, 3-, and 4-quantum signals increase with increasing τ_{MQ} . Spectra of samples with ^{13}C labels at methyl carbons of Ala21 and Ala30 are nearly identical. In unfibrillized samples (C), the 3-quantum amplitude is small and no 4-quantum signal is observed.

Figure 3. Comparison of experimental MQNMR amplitudes (black) with simulations for parallel (red), trimeric (green), dimeric (blue), and antiparallel organizations of β -sheets in A β_{1-40} fibrils, for samples labeled with ^{13}C at methyl carbons of Ala21 and Ala30. Experimental MQNMR amplitudes are normalized to a 1-quantum amplitude of 100. A logarithmic vertical scale is required because the amplitudes vary over two orders of magnitude. The parallel β -sheet model fits all of the experimental data most closely. Experimental amplitudes were determined from MQNMR spectra in Fig. 2 by integrating each subspectrum over the interval from -2 kHz to +3 kHz. Uncertainties in the experimental amplitudes, evaluated as the root-mean-squared noise integrated over a 5-kHz-wide interval, are ± 0.11 , ± 0.14 , and ± 0.14 for the Ala21-labeled A β_{1-40} fibril data, and ± 0.15 , ± 0.17 , and ± 0.24 for the Ala30-labeled A β_{1-40} fibril data, for $\tau_{\text{MQ}} = 4.8$ ms, 9.6 ms, and 14.4 ms, respectively.

Figure 4. The amino acid sequence of A β_{1-40} contains hydrophobic (black) and nonhydrophobic (red) residues. Ala21 and Ala30, sites that are shown by the MQNMR data to participate in parallel β -sheets, are colored green and blue, respectively. An in-register, parallel alignment of neighboring peptide chains in a β -sheet (top) juxtaposes the hydrophobic segments of neighboring chains, while an antiparallel alignment (bottom) does not. Hydrophobic interactions may dictate the β -sheet organization in A β_{1-40} fibrils.

References

1. Sipe, J. D. (1992) *Annu. Rev. Biochem.* **61**, 947-975.
2. Sunde, M. & Blake, C. C. F. (1998) *Quarterly Reviews of Biophysics* **31**, 1-39.
3. Chiti, F., Webster, P., Taddei, N., Clark, A., Stefani, M., Ramponi, G. & Dobson, C. M. (1999) *Proc. Natl. Acad. Sci. U. S. A.* **96**, 3590-3594.
4. Jimenez, J. L., Gujjarro, J. L., Orlova, E., Zurdo, J., Dobson, C. M., Sunde, M. & Saibil, H. R. (1999) *Embo J.* **18**, 815-821.
5. Blake, C. & Serpell, L. (1996) *Structure* **4**, 989-998.
6. Sunde, M., Serpell, L. C., Bartlam, M., Fraser, P. E., Pepys, M. B. & Blake, C. C. F. (1997) *J. Mol. Biol.* **273**, 729-739.
7. Fraser, P. E., Nguyen, J. T., Inouye, H., Surewicz, W. K., Selkoe, D. J., Podlisny, M. B. & Kirschner, D. A. (1992) *Biochemistry* **31**, 10716-10723.
8. Malinchik, S. B., Inouye, H., Szumowski, K. E. & Kirschner, D. A. (1998) *Biophys. J.* **74**, 537-545.
9. Serpell, L. C. & Smith, J. M. (2000) *J. Mol. Biol.* **299**, 225-231.
10. Glenner, G. G. & Wong, C. W. (1984) *Biochem. Biophys. Res. Comm.* **120**, 885-890.
11. Storey, E. & Cappai, R. (1999) *Neuropathol. Appl. Neurobiol.* **25**, 81-97.
12. Yankner, B. A. (1996) *Neuron* **16**, 921-932.
13. Gregory, D. M., Benzinger, T. L. S., Burkoth, T. S., Miller-Auer, H., Lynn, D. G., Meredith, S. C. & Botto, R. E. (1998) *Solid State Nucl. Magn. Reson.* **13**, 149-166.
14. Benzinger, T. L. S., Gregory, D. M., Burkoth, T. S., Miller-Auer, H., Lynn, D. G., Botto, R. E. & Meredith, S. C. (1998) *Proc. Natl. Acad. Sci. U. S. A.* **95**, 13407-13412.
15. Benzinger, T. L. S., Gregory, D. M., Burkoth, T. S., Miller-Auer, H., Lynn, D. G., Botto, R. E. & Meredith, S. C. (2000) *Biochemistry* **39**, 3491-3499.
16. Lansbury, P. T., Costa, P. R., Griffiths, J. M., Simon, E. J., Auger, M., Halverson, K. J., Kocisko, D. A., Hensch, Z. S., Ashburn, T. T., Spencer, R. G. S., Tidor, B. & Griffin, R. G. (1995) *Nat. Struct. Biol.* **2**, 990-998.
17. Halverson, K., Fraser, P. E., Kirschner, D. A. & Lansbury, P. T. (1990) *Biochemistry* **29**, 2639-2644.
18. Huang, T. H. J., Fraser, P. E. & Chakrabartty, A. (1997) *J. Mol. Biol.* **269**, 214-224.
19. Fraser, P. E., McLachlan, D. R., Surewicz, W. K., Mizzen, C. A., Snow, A. D., Nguyen, J. T. & Kirschner, D. A. (1994) *J. Mol. Biol.* **244**, 64-73.
20. Hilbich, C., Kisterswoike, B., Reed, J., Masters, C. L. & Beyreuther, K. (1991) *J. Mol. Biol.* **218**, 149-163.
21. Kirschner, D. A., Inouye, H., Duffy, L. K., Sinclair, A., Lind, M. & Selkoe, D. J. (1987) *Proc. Natl. Acad. Sci. U.S.A.* **84**, 6953-6957.
22. Tjernberg, L. O., Callaway, D. J. E., Tjernberg, A., Hahne, S., Lilliehook, C., Terenius, L., Thyberg, J. & Nordstedt, C. (1999) *J. Biol. Chem.* **274**, 12619-12625.
23. Lazo, N. D. & Downing, D. T. (1998) *Biochemistry* **37**, 1731-1735.
24. Chaney, M. O., Webster, S. D., Kuo, Y. M. & Roher, A. E. (1998) *Protein Eng.* **11**, 761-767.
25. Li, L. P., Darden, T. A., Bartolotti, L., Kominos, D. & Pedersen, L. G. (1999) *Biophys. J.* **76**, 2871-2878.
26. George, A. R. & Howlett, D. R. (1999) *Biopolymers* **50**, 733-741.
27. Yen, Y.-S. & Pines, A. (1983) *J. Chem. Phys.* **78**, 3579-3582.
28. Warren, W. S., Weitekamp, D. P. & Pines, A. (1980) *J. Chem. Phys.* **73**, 2084.

29. Baum, J., Munowitz, M., Garroway, A. N. & Pines, A. (1985) *J. Chem. Phys.* **83**, 2015.
30. Suter, D., Liu, S. B., Baum, J. & Pines, A. (1987) *Chem. Phys.* **114**, 103-109.
31. Tycko, R. (1999) *J. Magn. Reson.* **139**, 302-307.
32. Antzutkin, O. N. & Tycko, R. (1999) *J. Chem. Phys.* **110**, 2749-2752.
33. Weitekamp, D. P. (1983) in *Advances in Magnetic Resonance*, ed. Waugh, J. S. (Academic Press, New York), Vol. 11, pp. 111-274.
34. Roher, A. E., Lowenson, J. D., Clarke, S., Wolkow, C., Wang, R., Cotter, R. J., Reardon, I. M., Zurcherneeely, H. A., Henrikson, R. L., Ball, M. J. & Greenberg, B. D. (1993) *J. Biol. Chem.* **268**, 3072-3083.
35. Lansbury, P. T. (1992) *Biochemistry* **31**, 6865-6870.
36. Yamada, N., Ariga, K., Naito, M., Matsubara, K. & Koyama, E. (1998) *J. Am. Chem. Soc.* **120**, 12192-12199.
37. Bandekar, J. & Krimm, S. (1988) *Biopolymers* **27**, 909-921.
38. Shao, H. Y., Jao, S. C., Ma, K. & Zagorski, M. G. (1999) *J. Mol. Biol.* **285**, 755-773.
39. Sticht, H., Bayer, P., Willbold, D., Dames, S., Hilbich, C., Beyreuther, K., Frank, R. W. & Rosch, P. (1995) *Eur. J. Biochem.* **233**, 293-298.
40. Balbach, J. J., Ishii, Y., Antzutkin, O. N., Leapman, R. D., Rizzo, N. W., Dyda, F., Reed, J. & Tycko, R. (2000) *Biochemistry*, in press.
41. Jarrett, J. T., Berger, E. P. & Lansbury, P. T. (1993) *Biochemistry* **32**, 4693-4697.
42. Iwatsubo, T., Odaka, A., Suzuki, N., Mizusawa, H., Nukina, N. & Ihara, Y. (1994) *Neuron* **13**, 45-53.
43. Hasegawa, K., Yamaguchi, I., Omata, S., Gejyo, F. & Naiki, H. (1999) *Biochemistry* **38**, 15514-15521.

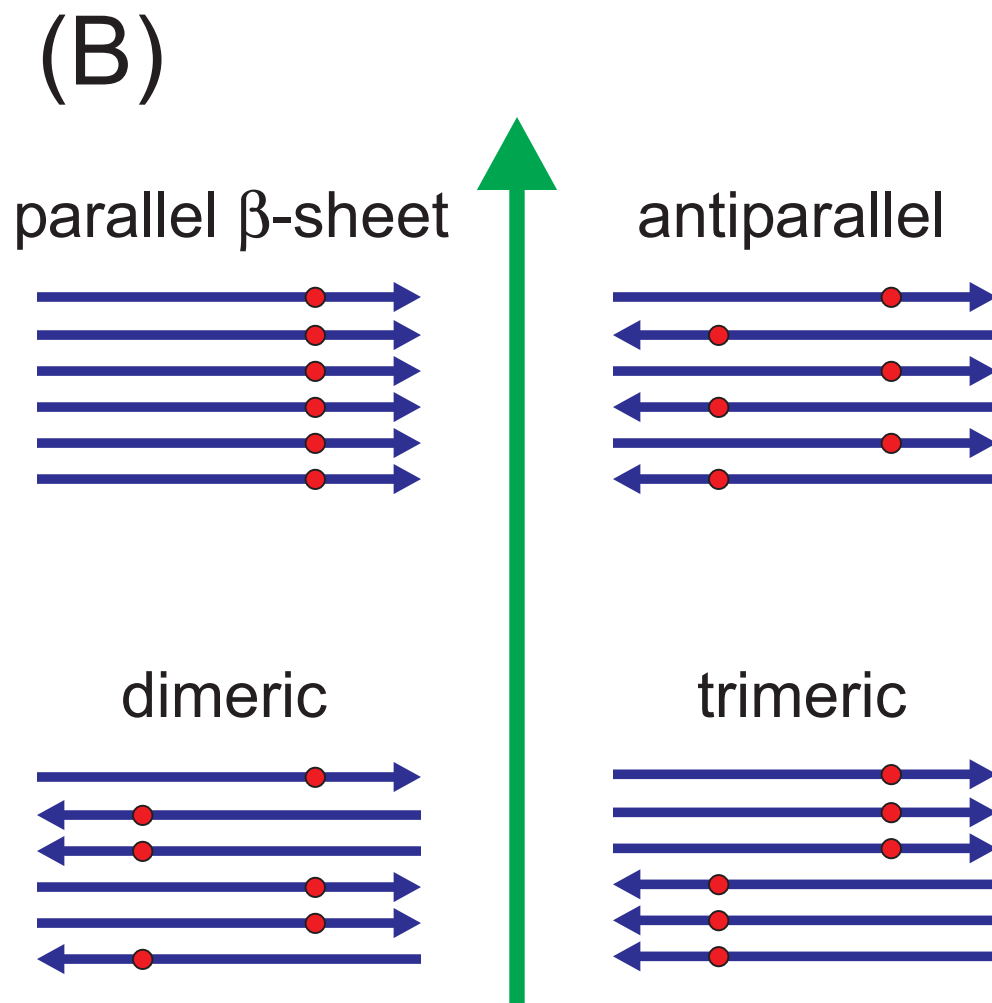
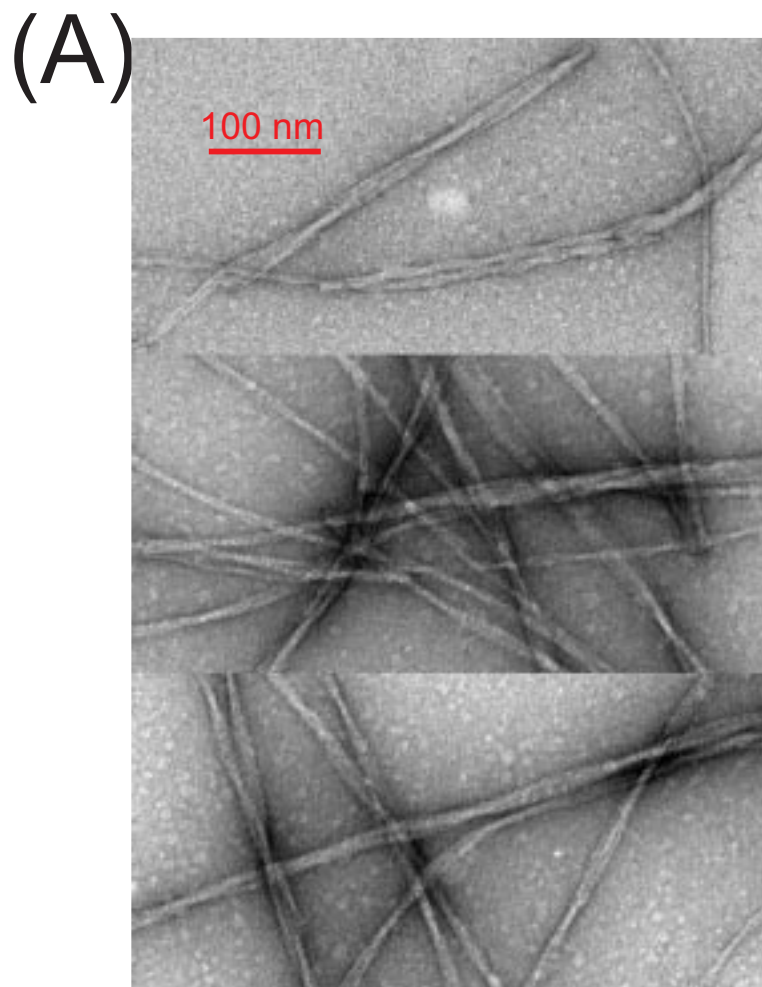


Figure 1, Antzutkin et al., "Multiple quantum solid state NMR ..."

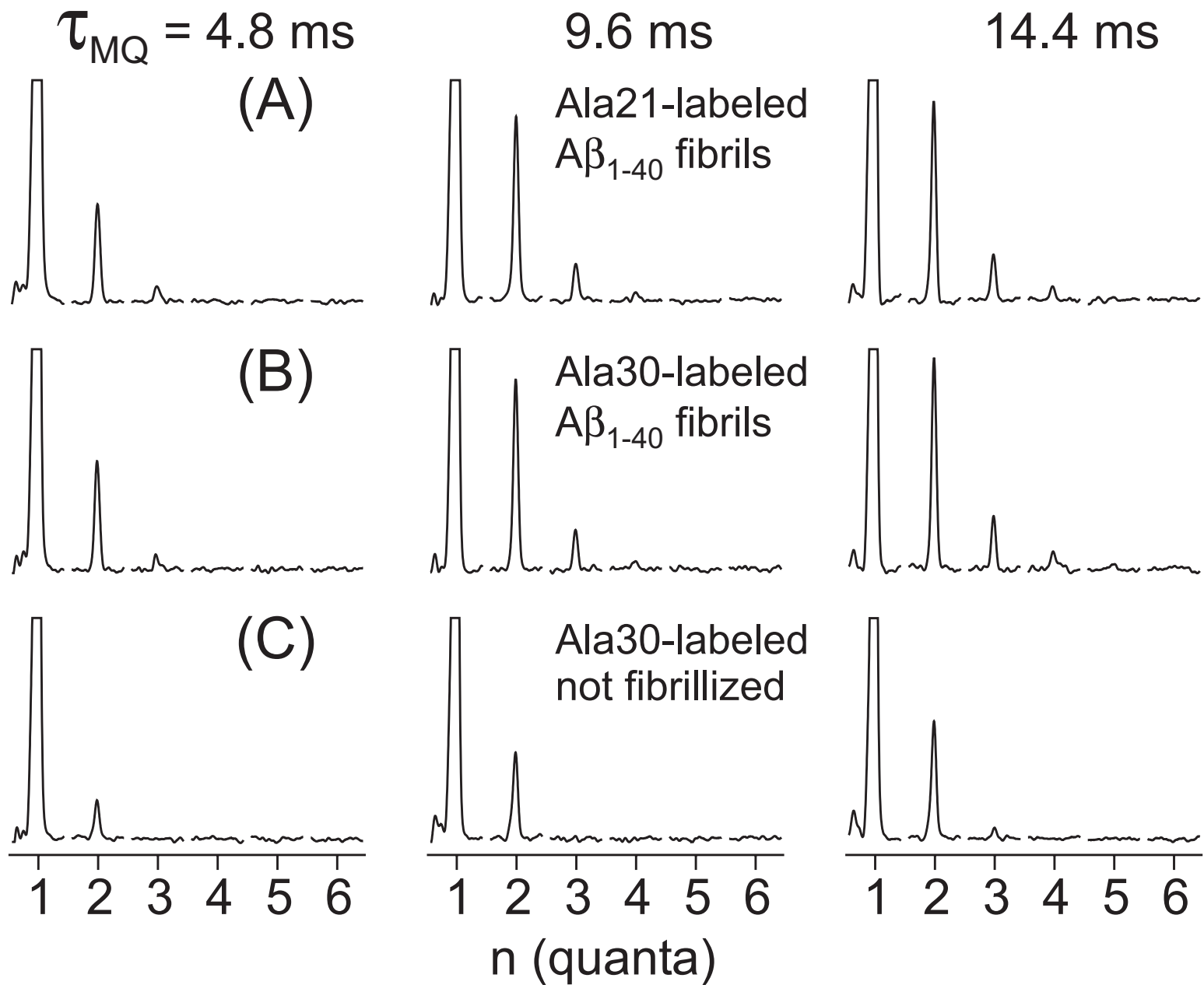


Figure 2, Antzutkin et al., "Multiple quantum solid state NMR ..."

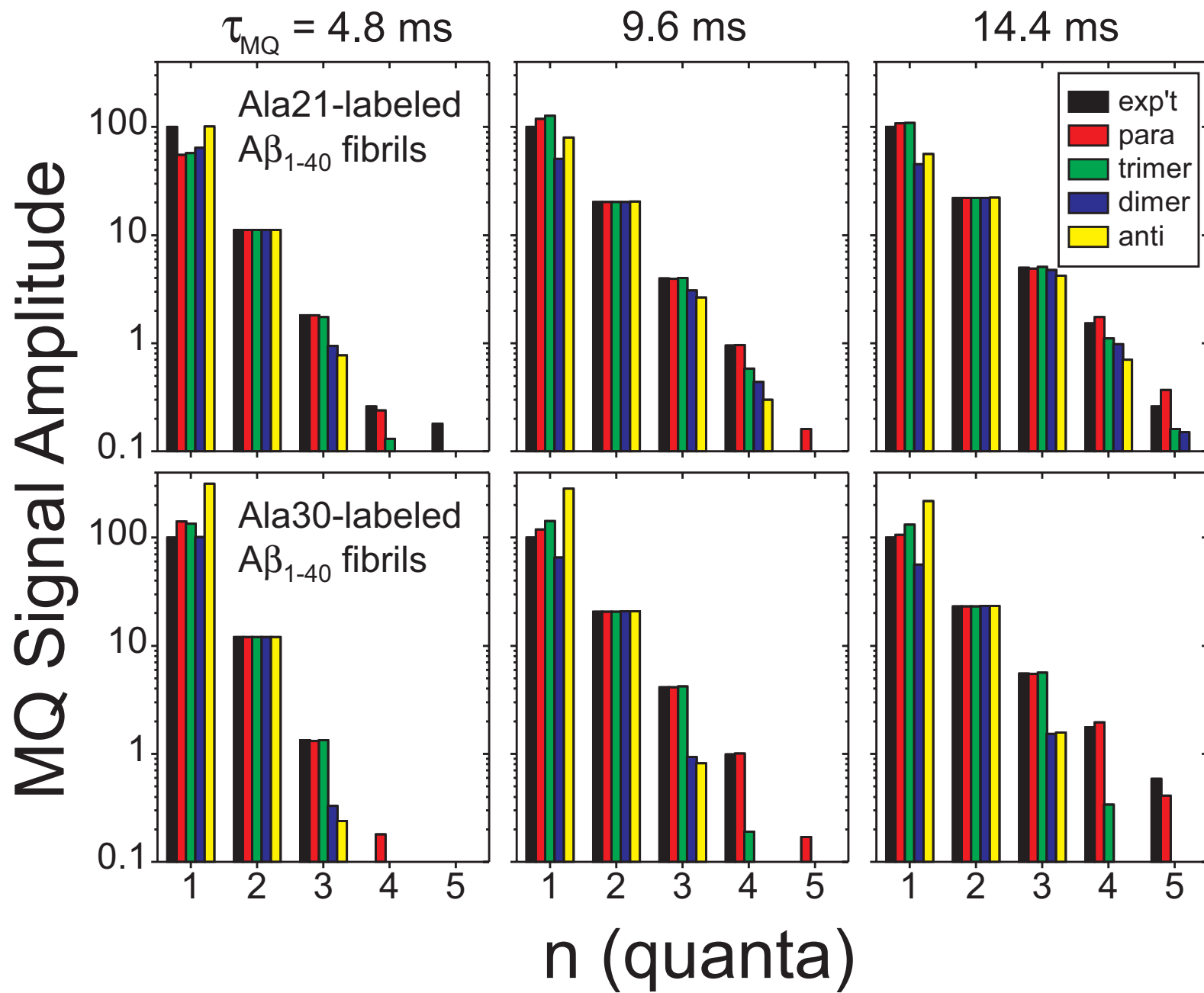


Figure 3, Antzutkin et al., "Multiple quantum solid state NMR ..."

1 10 20 30 40
 DAEFRHDSGYEVHHQKLVFFAEDVGSNKGAIIGLMVGGVV
 DAEFRHDSGYEVHHQKLVFFAEDVGSNKGAIIGLMVGGVV
 DAEFRHDSGYEVHHQKLVFFAEDVGSNKGAIIGLMVGGVV
 DAEFRHDSGYEVHHQKLVFFAEDVGSNKGAIIGLMVGGVV

 DAEFRHDSGYEVHHQKLVFFAEDVGSNKGAIIGLMVGGVV
 VVGGVMLGIIAGKNSGVDEAFFVLKQHHEVEYGSDFRFEAD
 DAEFRHDSGYEVHHQKLVFFAEDVGSNKGAIIGLMVGGVV
 VVGGVMLGIIAGKNSGVDEAFFVLKQHHEVEYGSDFRFEAD
 40 30 20 10 1

Figure 4, Antzutkin et al., "Multiple quantum solid state NMR ..."